Earth and Planetary Science Letters 296 (2010) 353–359

Contents lists available at ScienceDirect

Earth and Planetary Science Letters

journal homepage: www.elsevier.com/locate/epsl

Space/time coupling in brittle deformation at geophysical scales

David Marsan [a], Jérôme Weiss [b,*]

[a] LGIT, CNRS, Université de Savoie, Campus Scientifique, 73376 Le Bourget du Lac cedex, France
[b] LGGE, CNRS, Université J. Fourier, 54 rue Molière, BP 96, 38402 St Martin d'Hères Cedex, France

ARTICLE INFO

Article history:
Received 28 August 2009
Received in revised form 17 May 2010
Accepted 19 May 2010
Available online 15 June 2010

Editor: Y. Ricard

Keywords:
earthquakes
sea ice
fracture interactions

ABSTRACT

Strong intermittency as well as spatial heterogeneity characterize the brittle deformation of geophysical objects such as the Earth's crust or the Arctic sea-ice cover. They can be expressed through specific scaling laws, that relate, for a space–time domain, (a) the number of earthquakes or (b) the strain rate, vs. the size of the domain, for the Earth's crust or the Arctic sea ice, respectively. However, in both cases, spatial (respectively temporal) scaling depends on the time (respectively spatial) scale considered, i.e., the space and time scaling dependences are coupled. Here, we show that this space–time coupling of brittle deformation at geophysical scales can be summarized through a unique scaling law characterizing the discrete fracturing events (earthquakes or displacement events along sea-ice leads). As suggested by an analysis of southern Californian seismicity, we argue that this space–time coupling is likely to emerge from the complex correlation patterns related to chain triggering of earth- or ice-quakes.

1. Introduction

The brittle deformation of geophysical objects such as the Earth's crust or the Arctic sea-ice cover is characterized by intermittency as well as spatial heterogeneity, both expressed through specific scaling laws. For the Earth's crust, spatial heterogeneity is illustrated by the fractal clustering of earthquake hypocenters (Kagan and Knopoff, 1980; Kagan, 1991):

$$N(R) \sim R^D \tag{1}$$

where $N(R)$ is the number of hypocenters within a region of radius R, and $0 \leq D \leq 3$ is a fractal dimension. Intermittency, i.e. time clustering of events, is caused by earthquake interaction mechanisms, i.e., triggering of an earthquake by previous earthquakes. This triggering is illustrated by the Omori's law (Omori, 1894) that states that the rate of aftershocks triggered by a mainshock decays with time according to an inverse power of time, $1/t^p$. Alternatively, without considering the causal relationship implied by mainshock–aftershock triggering, this intermittency has been also expressed by fractal clustering (Kagan and Jackson, 1991):

$$N(t) \sim t^\delta \tag{2}$$

where $N(t)$ is the number of earthquakes within a time window of duration t, and $0 \leq \delta \leq 1$ is a fractal exponent. As shown below, relation (2) is probably in many cases an oversimplification of a more complex trend.

In case of the Arctic sea-ice cover, the much faster dynamics allow to directly observe the intermittency and spatial heterogeneity of deformation in terms of the scaling properties of strain-rate patterns. Using Lagrangian tracking of points on successive SAR satellite images (Fily and Rothrock, 1987; Kwok et al., 1990) or of ice-tethered buoys in order to derive strain-rate patterns, it was shown recently that the average sea-ice strain rate is characterized by spatial as well as temporal scaling laws (Marsan et al., 2004; Rampal et al., 2008). We define the total strain rate $\dot{\epsilon}$ as $\dot{\epsilon} = \varepsilon_{\mathrm{tot}}/t$, where $\varepsilon_{\mathrm{tot}} = \sqrt{\mathrm{shear}^2 + \mathrm{divergence}^2}$ is the total deformation occurring during a time interval t. The spatial scaling of this strain rate, i.e., the dependence of $\dot{\epsilon}$ on the size R of the domain, is given by:

$$\dot{\varepsilon}(R) \sim R^{-\beta} \tag{3}$$

where the exponent β expresses the degree of heterogeneity of sea-ice deformation, bounded by $\beta = 0$ for a homogeneous deformation field (e.g. viscous-like), and by $\beta = d$, the topological dimension, for a deformation localized along a single fracture ($d = 2$ for sea ice, see below). Similarly, the dependence of $\dot{\epsilon}$ on the observation time scale t is:

$$\dot{\varepsilon}(t) \sim t^{-\alpha} \tag{4}$$

where α is a measure of the degree of intermittence of the deformation process, bounded by $\alpha = 0$ for a non-intermittent viscous-like flow, and by $\alpha = 1$ for a deformation accommodated by a single cracking event.

* Corresponding author.
E-mail addresses: David.Marsan@univ-savoie.fr (D. Marsan), weiss@lgge.obs.ujf-grenoble.fr (J. Weiss).

0012-821X/$ – see front matter © 2010 Elsevier B.V. All rights reserved.
doi:10.1016/j.epsl.2010.05.019

However, observations reveal that these exponents D, β and δ, α that characterize the spatial heterogeneity and the intermittency of brittle deformation are not constant: instead, the two spatial exponents D and β depend on the time scale considered, whereas the temporal exponents δ and α depend on the spatial scale. For crustal seismicity, using the PDE worldwide catalog, Kagan (1991) reported a D-value of 1.2 at small time scales (1 day), which eventually reaches $D \approx 2.1$ at large time scales (25 years). This growth of D with time suggests a memory effect of the system that slowly weakens with time: starting with a given fracture/fault at time $t=0$, the initially strong spatial clustering implies that subsequent fractures/faults occurring quickly after $t=0$ will be observed close to the initial location. However, as time goes on, less and less can be said about the initiation of fractures nearby, which become more and more unconditioned on the initial position.

Similarly, for four worldwide and a regional (Californian) catalogs, Kagan and Jackson (1991) reported a δ-value around 0.2 for small spatial scales (10 km) and close to the limit value $\delta=1$ at very large scales ($>10^4$ km). This increase of δ illustrates a slow weakening of time correlations with increasing distance.

For Arctic sea ice, β decreases with increasing time scale, from $\beta=0.85$ for $t=3$ h to $\beta=0.35$ for $t\approx 2$ months in winter (respectively 0.85 for 3 h and 0.42 for 1 month, in summer) (Rampal et al., 2008). Sea-ice deformation appears more homogeneous as one considers a longer time scale, but localized deformation features persist over a season, in agreement with the analysis by Coon et al. (2007). Similarly, α decreases with increasing spatial scale, from $\alpha=0.89$ for $R\approx 1$ km to $\alpha=0.30$ for $R\approx 300$ km in winter (respectively 0.87 and 0.25 for summer): intermittency decreases as one averages deformation over a coarser spatial scale, although this intermittency persists even at large spatial scales, i.e. sea-ice deformation does not mimic viscous flow ($\alpha=0$) at scales significantly large compared to the size of the Arctic basin.

We will show in this paper that the dependence of D on t and δ on R in one hand, and of β on t and α on R on the other hand, are the two related aspects of a strong space/time coupling that characterizes brittle deformation. Since a similar coupling is observed for both the Earth's crust and the Arctic sea-ice cover, it suggests that it is characteristic of the brittle deformation of large geophysical objects.

2. Space/time coupling in the deformation of the Arctic sea-ice cover

The strain rate within a region of size R and a time window of duration t, scales according to Eqs. (3) and (4). This behaviour is obtained when analyzing the total deformation rate, hence a positive scalar which accounts for both shear strain as well as changes in surface. The dependence of exponent α (respectively β) on spatial scale (respectively time scale) implies that $\dot{\epsilon}(R,t)\sim t^{-\alpha(R)}\sim R^{-\beta(t)}$. This can be rewritten as

$$\dot{\epsilon}(R,t)\sim t^{-\alpha_0}R^{-\beta_0}e^{c\ln(t)\ln(R)} \tag{5}$$

which thus gives that $\dot{\epsilon}(R)\sim R^{(-\beta_0+c\ln(t))}$ hence $\beta(t)=\beta_0-c\ln(t)$, and $\dot{\epsilon}(t)\sim t^{(-\alpha_0+c\ln(R))}$ hence $\alpha(R)=\alpha_0-c\ln(R)$. Parameter c thus represents the strength of the space/time coupling, whereas α_0 and β_0 are constants which values depend on the chosen space and time units, and thus that have no particular physical meaning. The observed dependence of α on t and β on R for Arctic sea ice (Rampal et al., 2008) are in reasonable agreement with this expression, with $c\approx 0.10$ (Fig. 1).

The Arctic sea-ice cover deformation results from the opening, closing and shearing of the so-called 'leads', i.e. the fractures and faults that run through the entire ice thickness, and as such is mainly caused by brittle, fracturing events (Schulson, 2004; Weiss et al., 2007; Weiss and Schulson, 2009). A discontinuous model of motion was already

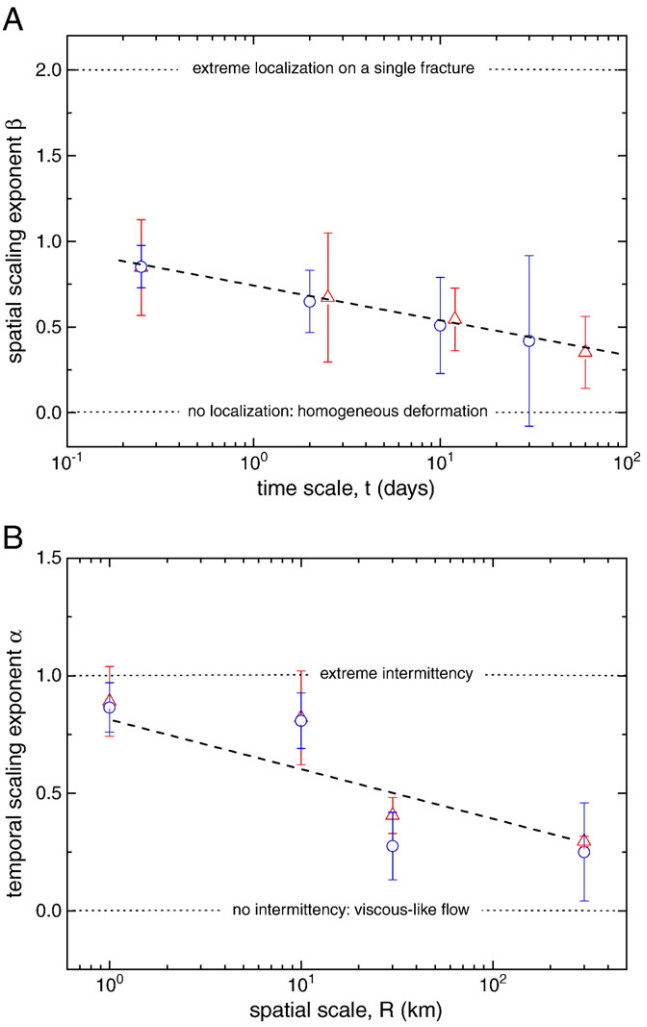

Fig. 1. Space–time coupling in Arctic sea-ice deformation. (A) Evolution of the spatial scaling exponent β, characterizing the spatial heterogeneity of Arctic sea-ice deformation, cf. Eq. (3), with the duration$t$ of the time window considered. Triangles: winter; circles: summer. See Rampal et al. (2008) for more details about the determination of β-values and the associated error bars. Exponent β decreases as $\beta\sim -c\times\ln(t)$ over the full scale range. The dashed line shows this trend with $c=0.10$. Large uncertainties on β imply that c is badly resolved, with a relative error of 90%. (B) Evolution of the temporal scaling exponent α, characterizing the intermittency of Arctic sea-ice deformation, cf. Eq. (4), with the spatial scale R. Triangles: winter; circles: summer. See Rampal et al. (2008) for more details about the determination of α-values and the associated error bars. The dashed line represents a logarithmic scaling $\alpha\sim -c\times\ln(t)$, with $c=0.10\pm 0.015$.

proposed by Thorndike (1986), to show how the collective effect of many fracturing leads can explain observations of sea-ice motion. This model was however based on crude hypotheses, such as a fully random (Poissonian) distribution of fracturing events in space and time, and a Gaussian distribution for the displacements across the leads. As shown below, some of these hypotheses disagree with observations and/or the scaling of the strain rate reported above (Eqs. (3) to (5)). We here elaborate on this seminal model, to investigate how the scaling expressed in Eq. (5) translates in terms of the number of fracturing events with region size R and observation time interval t.

Considering two points A and B distant by R, such as ice-tethered buoys, their relative displacement, or dispersion u (scaling laws (3) and (4) were obtained from dispersion rates of pairs of buoys (Rampal et al., 2008)), results from the cumulative effect of all the displacements $u_1,...,u_n$ at the n leads crossing the segment AB. Note that these displacements can be divergent, convergent, and/or transverse in any

direction of the fault, and their mean is assumed to be zero. This model amounts to neglect the elastic part of the deformation, an approximation that is reasonable as long as R is much greater than the thickness of the cover, i.e. a few meters on average. As is the case with crustal earthquakes, for which the magnitudes, hence the fault-averaged slip, are independent from one event to the next, we consider here that these displacements are all independent of each other — which does not mean that their occurrences (times and locations) are independent (see below). The dispersion u is given by the sum $\sum_{i=1}^{n} u_i$, and therefore scales as $n^{1/\gamma}$, where γ is an exponent equal to (if the individual displacements have a finite variance) or less than 2 (if the pdf of the displacements lies outside the Gaussian attractor basin, i.e. if the individual displacements have an infinite variance) (Sornette, 2000). Since (i) the strain rate is $\dot{\varepsilon}(R,t) = \frac{u}{R \times t}$ (Rampal et al., 2008), (ii) the scaling of $\dot{\varepsilon}(R,t)$ is as expressed in Eq. (5), and (iii) the number $N(R,t)$ of ice deformation events in a region of size R is the square of the number n of leads cutting across a segment of length R, we obtain that:

$$N(R,t) \sim t^{\delta_0} R^{D_0} e^{c' \ln(t) \ln(R)} \tag{6}$$

with $\delta_0 = 2\gamma(1-\alpha_0)$, $D_0 = 2\gamma(1-\beta_0)$, and $c' = 2\gamma c$. Eq (6) is, for lead-induced deformation events, the mirror expression of the coupled scaling law (5).

Considering either a time interval of fixed duration t, or a region of fixed size R, Eq. (6) implies that Eq. (1) and Eq. (2) also describe respectively the spatial heterogeneity and intermittency of sea-ice fracturing events, enlightening the analogy between the crust and the sea-ice cover. This also means that the occurrences of these events are not independent, in contradiction with the hypotheses of the original Thorndike's model. The value of parameter γ is not well constrained, but several arguments can be proposed in order to discuss a crude estimate. For crustal earthquakes, the seismic moment M is proportional to $M \sim u \times A$, where A is the rupture area. For large earthquakes that break the whole width of the schizosphere, M scales as u^2. A similar scaling is relevant for sea-ice leads, especially given the relatively small thickness of the ice cover. Assuming further that $M \sim 10^{(1.5 \times m)}$ (Hanks and Kanamori, 1979) where m is the magnitude, and that m is distributed according to the Gutenberg–Richter law $f(m) \sim 10^{-bm}$ where b is the so-called b-value, we obtain that the pdf of M is $f(M) \sim M^{-\left(1+\frac{2b}{3}\right)}$. This finally gives that $f(u) \sim u^{-\left(1+\frac{4b}{3}\right)}$, hence that $\gamma = \min\left\{2; \frac{4b}{3}\right\}$. Whereas the b-value for crustal seismicity is generally close to 1 (Utsu, 2002), i.e. $\gamma \approx 4/3$ in this case, the very scarce seismoacoustic data available for sea ice (Dudko et al., 1998) support the Gutenberg–Richter law with $b = 1.53 \pm 0.10$ (modified from Weiss, 2003), but is limited to very small, local ice-quakes corresponding to displacements u of the order of μm to mm (Dudko, 1999). We therefore need to be cautious with this estimate of the γ parameter from seismic data, which is clearly not well resolved. The existence of regional scale ice-quakes has still to be demonstrated. The scaling range of the equivalent of the Gutenberg–Richter law for these events is still unknown. The seismoacoustic observations are generally confined to small scale areas (up to 1 km), over short observation spans. Too little is known about the strain relaxation processes leading to these seismic events, which, as with crustal earthquakes, could possibly mix brittle and slow fracturing mechanisms. A b-value of 1.5 would yield that $4b/3 = 2$, hence $\gamma = 2$, i.e., the pdf of the displacements across individual leads would remain within the Gaussian attraction basin, as assumed by Thorndike (1986).

This estimation of γ, however, seems in contradiction with the observations of Lindsay and Rothrock (1995), who reported a power law distribution of lead widths w (or diverging displacements) from the analysis of radiometer (AVHRR) satellite images, $f(w) \sim w^{-1.6 \pm 0.1}$, i.e. a corresponding γ-value of 0.6 ± 0.1. Similar scaling has been reported for Earth's fault displacements (or slip), with a γ-value between 0.5 and 2 (Scholz and Cowie, 1990; Walsh et al., 1991; Otsuki, 1998). This disagreement confirms that the γ-value is still poorly constrained in case of sea-ice fracturing events. However, it is important to emphasize that this model is only intended to suggest that there exists a strong link between the two descriptions of sea-ice deformation, i.e. either through deformation fields as measured by buoy dispersion or satellite imagery, or through discrete events related to displacements across leads. As such, Eq. (6) shows that the coupled space–time scaling of the deformation rate of the Arctic sea-ice cover is equivalent to a coupled space–time scaling of the discrete ice-fracturing events occurring along the leads, as is also the case of crustal earthquakes. Indeed, the combination of Eqs. (1) and (2) derived from earthquake data, $N(R,t) \sim t^{\delta(R)} \sim R^{D(t)}$, can be rewritten as Eq. (6). This suggests that, for both the crust and the sea-ice cover, there exists a common mechanism that could explain this coupling.

From the D and δ values reported by Kagan (1991) and Kagan and Jackson (1991), the pertinence of Eq. (6) for worldwide crustal seismicity (PDE catalog, magnitude cut-off $m_c = 5.3$) can be tested (Fig. 2). Using $c' \approx 0.11$, a reasonable agreement is obtained, especially for the evolution of the fractal exponent δ with spatial scale. However, significant deviations from the proportionality of $D(t)$ with $\ln(t)$ are observed either towards small and large time scales. At time scales larger than 10^3 days (about 3 years), this might be interpreted as a vanishing space/time coupling, associated with an asymptotic value of $D(\infty) \approx 2.2$ characterizing the underlying fractal structure of the Earth's fault system (Kagan, 1991). Note that the δ-values plotted on Fig. 2B have been estimated by Kagan and Jackson (1991) over a time scale range from 1 to 10^3 days over which space/time coupling is expected to hold. Deviations observed towards small time scales are more difficult to interpret. Catalog incompleteness after large earthquakes and/or the spatial resolution of hypocenter location for this worldwide catalog may have an influence.

To better test the proposed coupled scaling law on seismicity data, we analyze in the next section a more recent regional catalog of southern California with an improved spatial resolution and a smaller magnitude cut-off ($m_c = 2.3$). We show that the fractal time clustering proposed by Kagan and Jackson (1991) is an oversimplification, but that an extended-scaling version of Eq. (6) well describes the data in a unified form. This analysis is then exploited in Section 4 to suggest that this coupling could emerge from the complex chain of triggering that characterizes seismicity dynamics.

3. Space/time coupling in a high resolution earthquake catalog

We revisit the analysis of earthquake space–time scaling coupling as previously evidenced by Kagan (1991) and Kagan and Jackson (1991), using a southern California earthquake catalog (Shearer et al., 2005) that covers 19 years of activity (1984 to 2002), and gives relocated hypocenter positions with a typical accuracy of less than 100 m. The magnitude of completeness is $m_c = 2.3$ when considering the whole 19-year period, although it experiences transient increases in the aftermath of large shocks. There are $N = 37{,}059$ $m \geq 2.3$ earthquakes. We consider distances to the fault rather than hypocentral distances: the distance between earthquake A and earthquake B is thus the nearest distance from the causative fault of A to the hypocenter of B. This computation is detailed in the supplementary information of Marsan and Lengliné (2008): the causative fault is modelled as (i) a point source for $m < 4$, (ii) a finite, square fault with length and width scaling with m according to $L = 10^{0.5(m-4)}$ (L in km) for $6 > m \geq 4$, (iii) a geometrically complex fault as imaged by rupture trace observation and slip inversions for $m \geq 6$. We first estimate the space–time coupling of this population of earthquakes, and then develop in Section 4 a tentative explanation for this coupling.

The temporal clustering exhibits two distinct regimes, for t less or greater than 2 days, see Fig. 3A. This break in scaling is highly significant: we compute the change in the Akaike information criterion

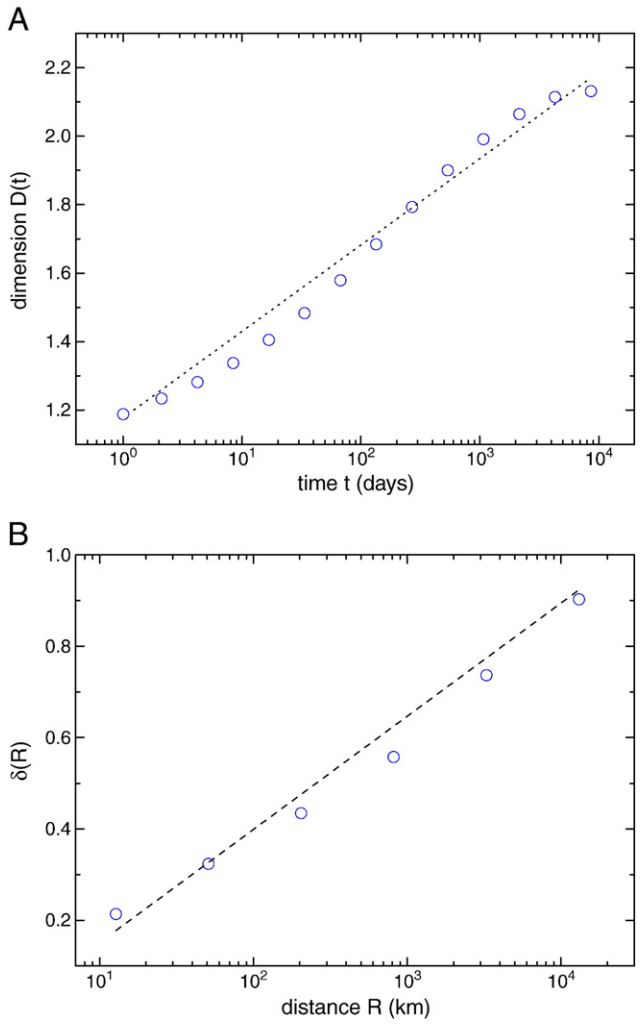

Fig. 2. Space–time coupling in crustal seismicity. (A) Evolution of the fractal dimension D, characterizing the spatial clustering of earthquake hypocenters $N(R) \sim R^D$, with the duration t of the time window considered. The plotted D-values are taken from (Kagan, 1991) for the shallow earthquakes (0–70 km) of the PDE worldwide catalog (magnitude cut-off $m_c = 5.3$). See Kagan (1991) for more details about the determination of D-values. The dashed line shows a logarithmic scaling $D \sim c' \times \ln(t)$, with $c' = 0.109 \pm 0.02$. (B) Evolution of the fractal exponent δ, characterizing the temporal clustering of earthquakes $N(t) \sim t^{\delta}$, with the size R of the region considered. The plotted δ-values are taken from (Kagan and Jackson, 1991) for the shallow earthquakes (0–35 km) of the PDE worldwide catalog. See Kagan and Jackson (1991) for more details about the determination of δ-values. The dashed line represents a logarithmic scaling $\delta \sim c' \times \ln(R)$, with $c' = 0.106 \pm 0.011$. Similar analyses performed on different catalogs (Harvard, DUDA, ABE) (Kagan and Jackson, 1991) give similar trends with slope c' varying from 0.10 to 0.13.

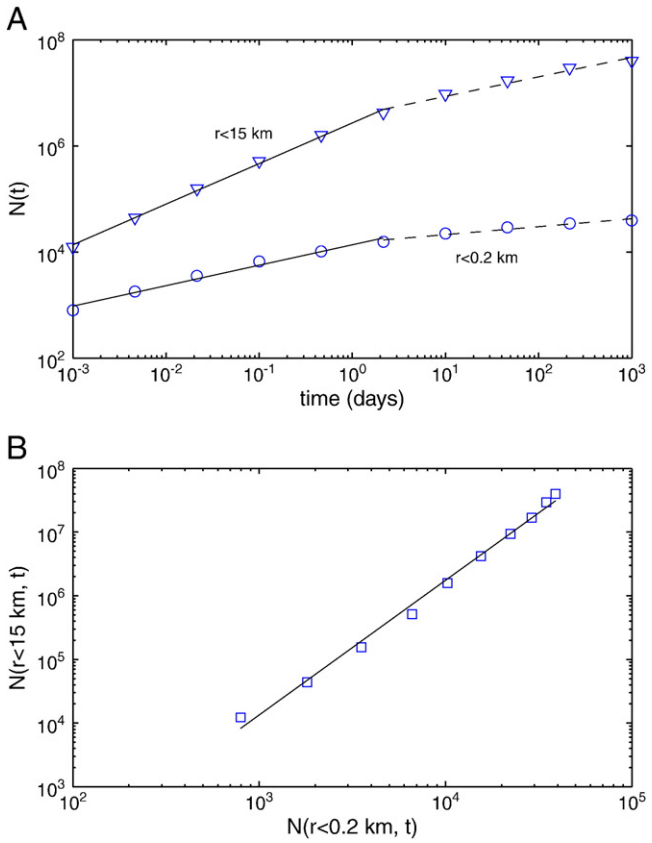

Fig. 3. Temporal clustering of the southern California earthquakes. (A) Number of pairs of earthquakes $N(R,t)$ separated by less than time t and distance R, function of t, for the two values of $R = 0.2$ km corresponding to the accuracy on the distances, and $R = 15$ km which is the thickness of the schizosphere. We observe two scaling regimes as depicted by a continuous and a dashed lines, that are separated by the transition scale $t = 2$ days. (B) $N(R = 15\text{ km}, t)$ vs. $N(R = 0.2\text{ km}, t)$. The power law relationship between the two expresses the fact that the exponents characterizing the two scaling regimes of Fig. 3A grows with R at the same relative rate.

(AIC) in order to compare the best model with one single scaling regime from 10^{-3} to 10^3 days, to the best model with two scaling regimes with a transition at 2 days (Main et al., 1999). We define $AIC = N\ln\left[\sum_{n=1}^{N}(y_n - \hat{y}_n)\right] + 2p$, where the N datapoints y are compared to the best fit $\hat{y}$ given the model, and p is the number of free parameters (either 2 or 4 depending on the case). We obtain that $\delta AIC = AIC(\textit{two regimes}) - AIC(\textit{single regime}) = -22.0$ for $r < 0.2$ km, and $\delta AIC = -26.2$ for $r < 15$ km. Despite this break in scaling, the exponents characterizing the two temporal regimes of $N(R,t)$ clearly increase with the size of the volume R. In fact, the relative increase λ of the two exponents is the same. This can be seen in Fig. 3B, which displays $N(R = 15\text{ km}, t)$ vs. $N(R = 0.2\text{ km}, t)$, for t ranging from 10^{-3} to 10^3 days, hence a very wide time scale interval. We obtain, to a very good accuracy, that $N(R = 15\text{ km}, t) \sim N(R = 0.2\text{ km}, t)^{\lambda}$, with $\lambda = 2.11$, whatever the temporal regime considered. Translated in terms of the dimension δ as with the analysis of Kagan and Jackson (1991), this exponent λ is equal to the ratio $\delta(R = 15\text{ km})/\delta(R = 0.2\text{ km})$. Fig. 4

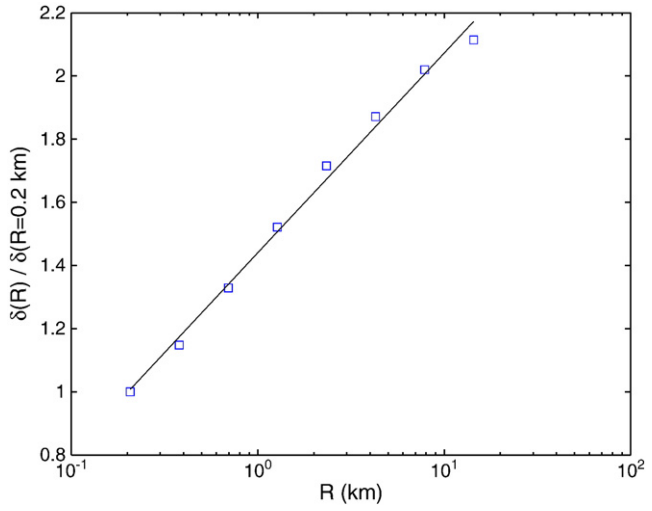

Fig. 4. Dependence of the temporal clustering on the spatial scale R. Ratio $\delta(R = 15\text{ km})/\delta(R = 0.2\text{ km})$ vs. R, for R ranging from 0.2 km to 15 km. The log-linearity of this ratio with R, as shown by the black line, implies that $\delta(R) = 0.27 \times \delta(R = 0.2\text{ km}) \times \ln(R)$. The relative uncertainty on the coupling value 0.27 is $\pm 12\%$.

shows these ratio when comparing $N(R,t)$ to $N(R=0.2\text{ km}, t)$, for R ranging from 0.2 km (resolution on the distances) to 15 km (thickness of the schizosphere). We find that $\delta(R)=0.27\times\delta(R=0.2\text{ km})\times\ln(R)$, hence a coupling coefficient $c'=0.27\times\delta(R=0.2\text{ km})$, cf. Eq. (6).

On the other hand, one single scaling regime characterize the spatial clustering, for 0.2 km$<R<$15 km, see Fig. 5A. We estimate the fractal dimensions $D(t)$, and plot them vs. time t in Fig. 5B. As expected, D increases with t, but, as in Fig. 3A, a clear change in trend is observed at about 2 days. This break is again very significant: $\delta AIC=-20.2$.

These results can be coherently summarized by the expression:

$$N(R,t)\sim\tau^{\delta_0}R^{D_0}e^{c'\ln(\tau)\ln(R)} \tag{7}$$

where $\tau=f(t)$ is a function of time that account for the transition scale at 2 days. This expression generalizes Eq. (6) to the present case with two distinct temporal regimes. Because of the functional τ of t, we cannot compare the new coupling coefficient c' with previous values inferred from the works by Kagan (1991) and Kagan and Jackson (1991). The latter assume that $\tau=t$, which we cannot validate with the present analysis. However, it is clear that a space–time coupling exists for this dataset, with a form very similar to the coupling described in Section 2, although the physical origin of this transition scale at 2 days remains unclear. This implies that the mechanism responsible for this space–time coupling is also present in this southern California data. We thus explore possible explanations for this coupling, by further analyzing this earthquake dataset.

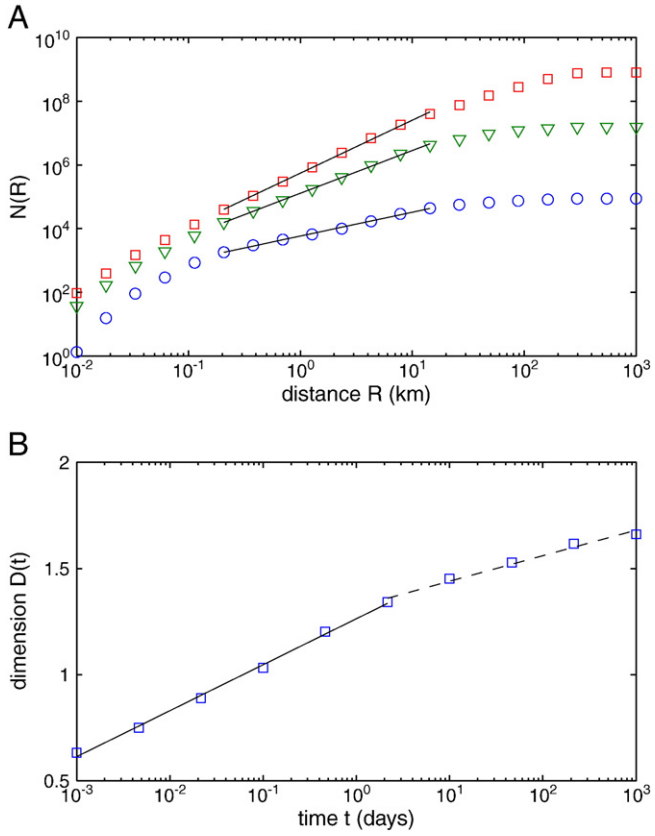

Fig. 5. Spatial clustering of the southern California earthquakes. (A) Number of pairs of earthquakes $N(R,t)$ separated by less than time t and distance R, function of R, for three values of t as indicated on the graph. A power law regime is found for R between 0.2 km and 15 km, as shown by the black lines. (B) Exponents D of the power law regime of a, vs. time t. The two regimes separated by $t=2$ days are shown with the two (continuous and dashed) lines.

4. Physical origin of the unified space/time coupling

Earthquakes trigger other earthquakes (aftershocks). Immediately following a mainshock, the earthquakes are more clustered together than during a 'normal' time interval taken at random. A first simple way of explaining the relaxation of spatial clustering with time is therefore to invoke two spatial clustering: (1) one that characterizes temporally correlated earthquakes, including aftershocks, $N_{\text{corr}}(R)\sim R^{D_{\text{coor}}}$, and (2) one that characterize the remaining, temporally uncorrelated earthquakes $N_{unc}(R)\sim R^{D_{uncr}}$, with $D_{unc}>D_{corr}$. Overall, clustering is dominated at short time scales by the 1st term, and at long time scales by the 2nd. From here on, we will use 'correlated' and 'uncorrelated' for 'temporally correlated' and 'temporally uncorrelated,' respectively. The simplest model comes from suggesting that $N(R,t)$ emerges from the sum of these two contributions:

$$N(R,t)=N_{corr}(R)N_{corr}(t)+N_{unc}(R)N_{unc}(t) \tag{8}$$

This model decouples space and time in the sense that the correlated and uncorrelated earthquake spatial distributions remain the same at all time scales. While it can explain the trend from strong to mild spatial clustering with increasing time scale, it is not appropriate: $N_{corr}(R,t)$ cannot be decoupled into $N_{corr}(R)N_{corr}(t)$. To prove this, we construct in Fig. 6 the sum of Eq. (8). The temporal terms are shown in Fig. 6A, by plotting $N(t)=N(R,t)$ vs. t for R infinitely large, and by compare it to $N_{unc}(t)$, which would be obtained in the case of a Poisson process, hence an earthquake time series only made of background events. We thus define the number of correlated pairs as $N_{corr}(t)=N(t)-N_{unc}(t)$. The uncorrelated earthquakes start dominating the rate $dN(t)/dt$ at about $t=100$ days. The two contributions $N_{corr}(R)N_{corr}(t)$ and $N_{unc}(R)N_{unc}(t)$ to $N(R,t)$ of Eq. (8) are shown in Fig. 6B and C, for $t=10^{-3}$ days (about 1 min 30 s) and for $t=10^{3}$ days (about 3 years). If the model expressed by Eq. (8) were correct, then (i) at short time scales (Fig. 6B) $N(R,t)$ and $N_{corr}(R)N_{corr}(t)$ should be equal, which, indeed, is true, and (ii) at long time scales (Fig. 6C) $N(R,t)$ and $N_{unc}(R)N_{unc}(t)$ should eventually become equal, which is not true. Instead, the strong clustering of the correlated pairs still dominates at short distances ($R<15$ km). This implies that $N_{corr}(R,t)$ cannot be simply decoupled into $N_{corr}(R)N_{corr}(t)$: the spatial clustering of correlated earthquakes becomes significantly milder with time.

The space–time coupling therefore originates from the evolution of the spatial distribution of correlated earthquakes. The fact that $D(t)$ increases quickly with time, even at $t\ll100$ days (Fig. 5) which marks the time at which the uncorrelated earthquakes start impacting the distribution, further indicates this.

Aftershocks can in turn trigger their own aftershocks, generating a cascade of triggering, hence of correlated earthquakes, that extends the initial aftershock pattern caused by the mainshock to longer durations and distances from the main fault. It is convenient to represent this cascade of triggering by a tree in which any earthquake A preceding earthquake B is either (1) the parent, i.e., A directly triggered B, (2) an ancestor, i.e., there exists a chain of parents–children leading from A to B, (3) a cousin, i.e., A and B have a common ancestor, or (4) not related to B, i.e., they have no common ancestor. Earthquakes can be grouped in clusters, with all earthquakes belonging to a cluster being either cousins, parents or ancestors of each other. The earliest earthquake of the cluster, having by definition no parent, is a so-called background earthquake. Fig. 7 shows an example of the various relationships between earthquakes. Earthquakes belonging to the same cluster are (temporally) correlated, while they are (temporally) uncorrelated otherwise. The spatial distribution of correlated earthquakes can therefore be studied if the triggering chain is correctly sorted out.

We use a recently proposed declustering procedure (Marsan and Lengliné, 2008, in press) to estimate the triggering chain of Californian earthquakes. This method computes the probability ω_{AB} that A could have directly triggered B, for all earthquake pairs, based on an

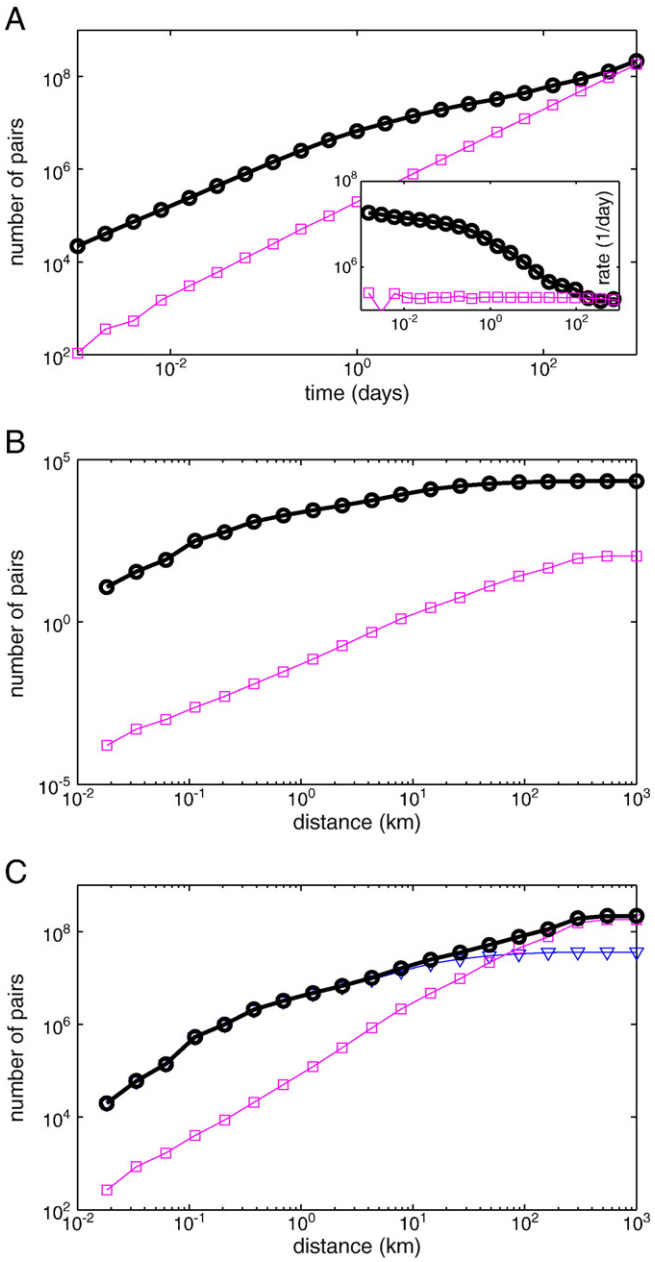

Fig. 6. Testing a model that decouples space and time. (A) Number of pairs of earthquakes $N(t)$ separated by less than time t (thick line) compared to the same if the time series were a realization of a Poisson process (thin line). The difference between the two corresponds to the correlated number of pairs $N_{corr}(t)$. Inset: corresponding rates of earthquakes. The uncorrelated regime becomes dominant at about $t=100$ days. (B) Number of pairs of earthquakes separated by less than time $t=10^{-3}$ days (about 1 min and 30 s) and distance R. Thin line: $N_{unc}(R,t=10^{-3}$ days) extrapolated from $N_{unc}(R,t=10^{3}$ days), by multiplying the latter by 10^6. Thick line: $N(R,t)$ as given by Eq. (8). At this time scale, $N(R,t)$ is dominated by $N_{corr}(R,t)$, the two terms being indistinguishable on this plot. (C) Same as B, for $t=10^3$ days. $N_{corr}(R,t=10^3$ days) (triangles) is extrapolated from $N_{corr}(R,t=10^{-3}$ days) $=N(R,t=10^{-3}$ days) using the analysis of A. The thick line (Eq. (8)) should follow $N_{unc}(R,t)$ (squares) at this time scale (10 times greater than the 100 days transition scale, see inset of A) if the model were correct.

Expectation–Maximization inversion algorithm (Dempster et al., 1977). Using these probabilities ω_{AB}, we can randomly draw realizations of the causal chain that links every earthquake to a single parent earthquake: earthquake B will then be a direct aftershock of earthquake A in ω_{AB} realizations of the causal chain, on average. For each realization of the causal chain, we separate the earthquakes into clusters of cousins. Repeating this for a great number of chain

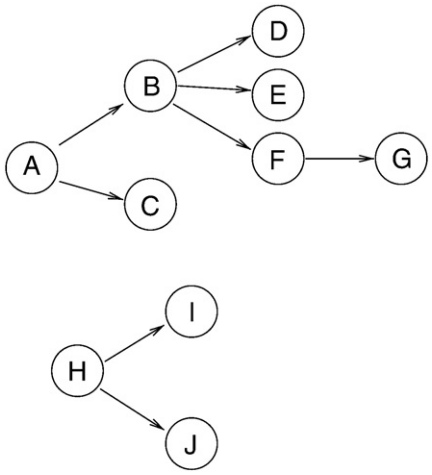

Fig. 7. Sketch of the possible relationships between earthquakes. In this example, A and H initiates two separate groups (clusters). Therefore, earthquake pairs made of elements belonging to the two groups (i) A,..., G and (ii) H, I, J, are uncorrelated. A is the parent of B and C, while it is the ancestor of D,..., G. B and C are cousins (they have a common ancestor, A, as are all the earthquakes of a given cluster (A to G on one side, H, I and J on the other side).

realizations, we estimate ω_{AB} the probability that A and B belong to the same cluster. This allows to compute $N_{cor}(R,t)$ as

$$N_{corr}(R,t) = \sum_{A,B\,/\,r_{AB}<R\,\&\,t_B-t_A<t} \Omega_{AB}$$

as well as the number of directly triggered earthquakes (aftershocks) $N_{trig}(R,t)$ function of R and t, as

$$N_{trig}(R,t) = \sum_{A,B\,/\,r_{AB}<R\,\&\,t_B-t_A<t} \omega_{AB}$$

Fig. 8 compares these two quantities, for $t=10^{-2}$ and 10^2 days. First, $N_{cor}(R,t)$ follows a power law in the 0.2–15 km interval, with an exponent D very close to the one shown in Fig. 5: $D=0.80$ compared to 0.82 for $t=10^{-2}$ days, and $D=1.39$ compared to 1.56 for $t=10^2$ days. For the latter time scale, the uncorrelated seismicity becomes effective in contributing to the spatial distribution, and the

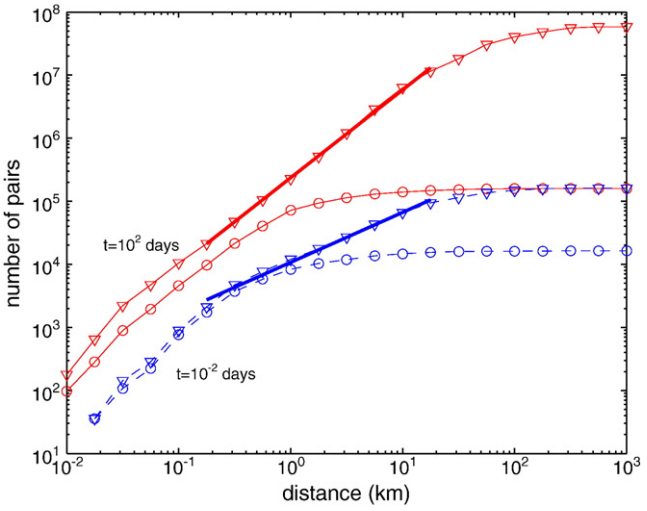

Fig. 8. Comparing the temporal evolution of spatial clustering of direct aftershocks and of correlated earthquakes. Number of pairs of earthquakes separated by less than distance R, and less than $t=10^{-2}$ days (two lower, dashed curves) or $t=10^2$ days (two upper, continuous curves). Circles: $N_{trig}(R,t)$. Triangles: $N_{cor}(R,t)$. The best power law fits for $N_{cor}(R,t)$ in the interval 0.2 km$<R<$15 km are shown in thick lines, yielding $D=0.80$ and $D=1.39$ respectively.

difference in the estimate of D is likely to come from the fact that this contribution is by definition ignored in $N_{cor}(R,t)$. This shows that (i) our estimate of $N_{cor}(R,t)$ is indeed correct, and (ii) $N(R,t)$ can be well approximated by $N_{cor}(R,t)$ at least for $t \ll 100$ days, and even to a relatively good accuracy for $t = 100$ days.

Second, the overall shape of $N_{trig}(R,t)$ evolves very little with t, and is clearly not a power law of R in the 0.2–15 km interval. This indicates that the spatial pattern of direct aftershocks is strongly clustered at short distances, and that it remains so at all time scales. Therefore, this suggests that the entire cascade of triggering, and not only direct triggering of aftershocks, is responsible for the space–time coupling described in Section 3. This is coherent with the fact that this cascade has been proposed to be responsible for a significant — although slow — diffusion of the aftershock distribution (Marsan and Lengliné, 2008; Helmstetter et al., 2003).

5. Conclusions

Because of mechanical interactions, (earth- or ice-) fracturing occurrences are correlated together. As a result, the brittle deformation of the Earth's crust and of the Arctic sea-ice cover exhibits clustering in space and in time, that can be expressed by power laws over specific scale intervals. The two ways to analyze deformation processes, either from a discrete point of view (quakes) or from continuous fields (SAR or buoy displacements), can be compared to each other. To do so, a crude but realistic model was developed in Section 2 to translate the strain-rate dependence of the Artic sea-ice cover on the scale of observation into an equivalent dependence for the discrete, lead-induced deformation events.

In both instances, the space–time clustering is characterized by a significant coupling: the spatial clustering decays (logarithmically when expressed with the fractal dimension D) with time, while the temporal clustering decays (also logarithmically) with the size of the region. This space–time coupling of the scaling dependence of the deformation is very similar in both cases, and it can therefore be seen as a rather general feature of two (large) geophysical objects in the brittle regime, that can be summarized into a unified scaling law.

A common mechanism that can explain the similarity of the space–time coupling of ice deformation and crustal earthquakes has been tested in Section 4. We propose that this feature emerges from the cascade of earth-/ice-event triggering that, for the crust, is known to extend the influence of earthquakes to longer durations and larger areas than just their own aftershock sequence. While this type of cascade process has already been proposed to characterize crustal earthquakes, we here suggest that it is also at work for the sea-ice cover. The collective dynamics of brittle (earth- or ice-) events manifests itself in this non-trivial space–time coupling, which goes well beyond a simple relaxation from a highly-clustered 'after-quake' initial distribution to a denser, hence less clustered, 'background' state. As this unified space–time coupled scaling encompasses the more specific temporal and spatial scaling laws, Eqs. (1) to (4) can be seen also as consequences of this cascading process.

Acknowledgments

We thank I. Main as well as another anonymous reviewer whose comments greatly helped improving the clarity of this manuscript on several points.

References

Coon, M., Kwok, R., Levy, G., Pruis, M., Schreyer, H., Sulsky, D., 2007. Arctic ice dynamics joint experiment (AIDJEX) assumptions revisited and found inadequate. J. Geophys. Res. 112, C11S90.
Dempster, A.P., Laird, N., Rubin, D.B., 1977. Maximum likelihood from incomplete data via the EM algorithm. J. Royal Stat. Soc. B 39, 1–38.
Dudko, Y.V., 1999. Analysis of Seismo-acoustic Emission from Ice Fracturing Events during SIMI'94. Massachusetts Institute of Technology.
Dudko, Y.V., Schmidt, H., von der Heydt, K., Scheer, E.K., 1998. Edge wave observation using remote seismoacoustic sensing of ice events in the Arctic. J. Geophys. Res. 103, 21,775–21,781.
Fily, M., Rothrock, D.A., 1987. Sea ice tracking by nested correlations. IEEE Trans. Geosci. Remote Sens. 25, 570–580.
Hanks, T.C., Kanamori, H., 1979. A moment magnitude scale. J. Geophys. Res. 84, 2348–2350.
Helmstetter, A., Ouillon, G., Sornette, D., 2003. Are aftershocks of large californian earthquakes diffusing? J. Geophys. Res. 108, 2483.
Kagan, Y.Y., 1991. Fractal dimension of brittle fracture. J. Nonlinear Sci. 1, 1–16.
Kagan, Y.Y., Jackson, D.D., 1991. Long-term earthquake clustering. Geophys. J. Int. 104, 117–133.
Kagan, Y.Y., Knopoff, L., 1980. Spatial distribution of earthquakes: the two point correlation function. Geophys. J. R. Astron. Soc. 62, 303–320.
Kwok, R., Curlander, J., McConnell, R., Pang, S., 1990. An ice motion tracking system at the Alaska SAR facility. IEEE J. Ocean. Eng. 15, 44–54.
Lindsay, R.W., Rothrock, D.A., 1995. Arctic sea ice leads from advanced very high resolution radiometer images. J. Geophys. Res. 100, 4533–4544.
Main, I.G., Leonard, T., Papasouliotis, O., Hatton, C.G., Meredith, P.G., 1999. One slope or two? Detecting statistically-significant breaks of slope in geophysical data, with application to fracture scaling relationship. Geophys. Res. Lett. 26, 2801–2804.
Marsan, D., Lengliné, O., 2008. Extending earthquakes' reach through cascading. Science 319, 1076–1079.
Marsan, D., Lengliné, O., in press. A new estimation of the decay of aftershock density with distance to the mainshock. J. Geophys. Res. doi:10.1029/2009JB007119.
Marsan, D., Stern, H., Lindsay, R., Weiss, J., 2004. Scale dependence and localization of the deformation of arctic sea ice. Phys. Rev. Lett. 93, 178,501.
Omori, F., 1894. On the aftershocks of earthquakes. J. Coll. Sci. Imp. Univ. Tokyo 7, 111–120.
Otsuki, K., 1998. An empirical evolution law of fractal size frequency of fault population and its similarity law. Geophys. Res. Lett. 25, 671–674.
Rampal, P., Weiss, J., Marsan, D., Lindsay, R., Stern, H., 2008. Scaling properties of sea ice deformation from buoy dispersion analyses. J. Geophys. Res. 113, C03002.
Scholz, C.H., Cowie, P.A., 1990. Determination of total strain from faulting using slip measurements. Nature 346, 837–839.
Schulson, E.M., 2004. Compressive shear faults within the arctic sea ice: fracture on scales large and small. J. Geophys. Res. 109, C07016. doi:10.1029/2003JC002108.
Shearer, P., Hauksson, E., Lin, G., 2005. Southern California hypocenter relocation with waveform cross-correlation, part 2: results using source-specific station terms and cluster analysis. Bull. Seism. Soc. Am. 95, 904–915.
Sornette, D., 2000. Critical Phenomena in Natural Sciences. Springer, Berlin.
Thorndike, A.S., 1986. Kinematics of sea ice. In: Untersteiner, N. (Ed.), The Geophysics of Sea Ice. Plenum Press, New York, pp. 489–549.
Utsu, T., 2002. Statistical features of seismicity. In: Lee, W.H.K., Kanamori, H., Jennings, P.C., Kisslinger, C. (Eds.), International Handbook of Earthquake and Engineering Seismology 81-A, Academic Press, pp. 719–732.
Walsh, J., Watterson, J., Yielding, G., 1991. The importance of small-scale faulting in regional extension. Nature 351, 391–393.
Weiss, J., 2003. Scaling of fracture and faulting in ice on Earth. Surv. Geophys. 24, 185–227.
Weiss, J., Schulson, E.M., 2009. Coulombic faulting from the grain scale to the geophysical scale: lessons from ice. J. Phys. D 42, 214017.
Weiss, J., Schulson, E.M., Stern, H.L., 2007. Sea ice rheology from in-situ, satellite and laboratory observations: fracture and friction. Earth Planet. Sci. Lett. 255, 1–8.